IEEJ Transactions on xx
Vol.xxx No.1 pp.1–8 DOI: 10.1541/ieejxxs.xxx.1

**Paper**

# Minimum-Variance Load-Side External Torque Estimation Robust Against Modeling and Measurement Errors

Shota Yamada*a) Student Member, Hiroshi Fujimoto* Senior Member

Sensorless external torque estimation is important for industrial applications. The load-side torque in a two-inertia system with a load-side encoder can be estimated by using either of the two observers that present different levels of robustness against modeling and measurement errors on the motor side and transmission part. By combining these observers, we propose a load-side external torque observer with high estimation accuracy even under modeling and measurement errors. Analyses of the observer with and without a joint torque sensor unveil the advantages and limitations of applying a joint torque sensor for external torque estimation. In addition, we derive a systematic design method for the proposed observers to minimize the estimation variance by considering the variance of the plant parameters and sensor measurements. The advantages of the proposed method are evaluated through simulations and experiments.

**Keywords:** Estimation, force sensing, reaction force observer, torque sensing, two-inertia system, two-mass system.

## 1. Introduction

Accurate force/torque detection is gathering notable research interest [1]. For example, Yamada *et al*. [2] estimate the cutting force for monitoring a machining process, whereas Ohba *et al*. [3] estimate the force to control an injection molding machine, and Katsura *et al*. [4] and Mitsantisuk *et al*. [5] estimate contact forces for control considering external environments. Likewise, force estimation is required to enable haptic applications [6–8].

The high cost of force/torque sensors and their induced reduction of resonance frequency of controlled systems make the use of sensorless force/torque estimation a promising alternative [9]. One of the most widely used sensorless estimation methods is the reaction force observer proposed in [10]. However, its estimation performance is degraded when a rigid body model is applied to resonant plants such as geared robots and ball-screw stages of machine tools [2]. Accurate force/torque estimation requires the careful consideration of resonant dynamics.

A plant with a resonant mode can be modeled as a two-inertia system [11], as illustrated in the block diagram of Fig. 1(a), and whose variables are defined in Table 1. Subscripts $M$ and $L$ denote the motor and load, respectively. For motion control with external environment interaction, external torque $d_L$ and not joint torque $T_s$ should be estimated, as the latter can be measured using joint torque sensors. Load-side inertia moment $J_L$ and viscosity $D_L$ should be considered for external torque estimation even when using joint torque sensors. Since a lot of torque sensors with high bandwidth are recently applied to cooperative robots (see e.g., [12]), we consider load-side external torque estimation in both cases where the system has a joint torque sensor or no joint torque sensor.

a) Correspondence to: yamada.shota13@ae.k.u-tokyo.ac.jp
* The University of Tokyo
5-1-5, Kashiwanoha, Kashiwa, Chiba 277-8561, Japan

Table 1. Definition of plant parameters variables.

| | | | |
|---|---|---|---|
| Inertia moment | $J$ | Motor torque | $T_M$ |
| Viscosity coefficient | $D$ | External torque | $d_L$ |
| Torsional rigidity | $K$ | Joint torque | $T_s$ |
| Angular velocity | $\omega$ | Torsional angle | $\theta_s$ |
| Motor-side disturbance | $d_M$ | | |

Recently, machine tools are equipped with linear encoders to obtain precise positioning at the load side even under nonlinearity and resonance in ball-screw mechanisms. Likewise, we expect an increasing adoption of load-side encoders in robotics and various industrial devices. In fact, we have proposed and evaluated a novel structure for industrial robots with load-side encoders [13]. Therefore, the estimation method using load-side encoder information is applicable to industrial devices, and the proposal of the effective estimation method is highly required.

For accurate estimation in two-inertia systems, two kinds of load-side external torque observers using load-side information are proposed. Matsuoka *et al*. [14] propose the arm disturbance observer that relies on load-side accelerometers. The difference between torque observer and disturbance observer depends on whether friction is subtracted from the output, as the latter observer compensates disturbance including friction. In this paper, we focus on accurate torque estimation without friction. Suzuki *et al*. [15] propose another observer using a position sensitive device to measure the torsional angle. In both observers, load-side external torque $d_L$ is estimated from joint torque $T_s$ and the torque obtained by an inverse load-side model and load-side velocity as follows:

$$\hat{d}_L = (J_{Ln}s + D_{Ln})\omega_L - T_s, \tag{1}$$

where $_n$ and $\hat{}$ indicate nominal and estimated variables, respectively. The observers differ in the estimation of joint torque $T_s$. In [14], joint torque $\hat{T}_{sM}$ is estimated from the motor-side dynamics and encoder using the law of action and reaction as follows:

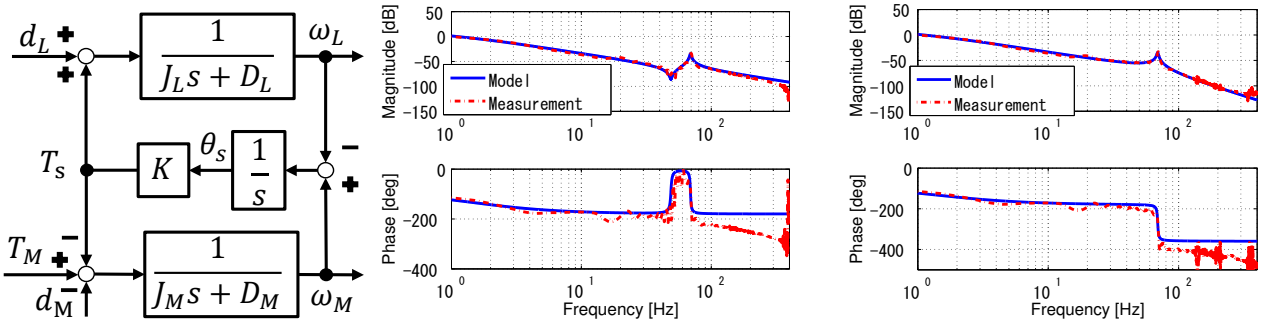


(a) Block diagram of a two-inertia system. (b) Frequency responses from the motor torque to the motor angle. (c) Frequency responses from the motor torque to the load angle.

Fig. 1. Block diagram and frequency responses of the two-inertia system motor bench.

$$\hat{T}_{sM} = (J_{Mn}s + D_{Mn})\omega_M - T_M - d_M. \tag{2}$$

Motor torque $T_M$ is measurable by a current sensor and considering motor disturbance $d_M$, which mainly comprises the motor-side friction that can be measured beforehand. We call this approach motor-side estimation as it uses the motor-side dynamics. On the other hand, in [15], joint torque $\hat{T}_{sK}$ is estimated from torsional information as follows:

$$\hat{T}_{sK} = \theta_s K_n. \tag{3}$$

where torsional angle $\theta_s$ can be measured using both the motor-side and load-side encoders or a position sensitive device. This approach avoids the friction modeling error of $(D_{Mn} \cdot \omega_M)$ and $d_M$ in (2). However, the value of $\hat{T}_{sK}$ can be deteriorated by the modeling error of torsional rigidity and nonlinearities in transmission mechanisms [16]. We call this approach transmission-part estimation. Nonlinearities exist in transmission mechanisms, but we unmodel the nonlinearities given their diversity and complexity [17, 18]. Instead, our proposed observer can mitigate the influence of nonlinearities. In conventional studies, either of the two estimation methods are selected depending on the system. For instance, in series elastic actuators equipped with well-identified linear springs, transmission-part estimation is preferred [19,20]. Also, when the system has a joint torque sensor, the joint torque can be obtained with robustness against modeling errors but sensitivity to measurement noise. We denote the joint torque obtained from a sensor as $T_{sS}$ and call the load-side external torque estimation using this measurement as torque-sensor-based estimation.

We propose accurate load-side external torque estimation that is robust against modeling and measurement errors by combining the estimation methods proposed in [14] and [15], specifically the estimated $\hat{T}_{sM}$, $\hat{T}_{sK}$, and $T_{sS}$ considering the availability of a joint torque sensor. Such combination is not novel, as Mitsantisuk *et al.* [21] use both methods for estimation, by calling the equation (2) multi-encoder disturbance observer and the equation (3) load-side disturbance observer. However, they define these observers for identification of the torsional rigidity by comparing their estimated values, assuming that the multi-encoder disturbance observer returns the true value. Likewise, both methods are combined in other approach by employing different frequency ranges to enhance the estimation bandwidth [22]. We introduce novel gains determining the ratio between the motor-side estimation and the transmission-part estimations and the joint torque by the torque sensor in the same frequency range to improve the robustness against modeling and measurement errors. Although these gains can be manually adjusted, we derive a systematic design method for the gains to minimize the variance of the estimated load-side external torque.

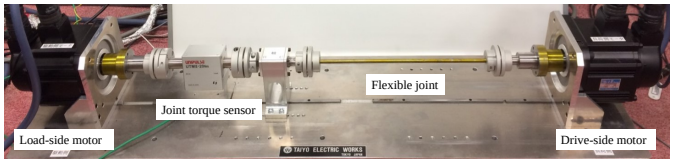


Fig. 2. Outlook of the two-inertia system motor bench.

Table 2. Parameters of the two-inertia system motor bench.

| | | |
|---|---|---|
| Motor-side inertia moment $J_M$ | 1.03e-3 | kg· m$^2$ |
| Motor-side viscosity coefficient $D_M$ | 8.00e-3 | N·m·s/rad |
| Torsional rigidity $K$ | 99.0 | N·m/rad |
| Load-side inertia moment $J_L$ | 8.70e-4 | kg·m$^2$ |
| Load-side viscosity coefficient $D_L$ | 1.71e-3 | N·m·s/rad |

The main contributions of this study are threefold:

(1) robustness enhancement of load-side external torque estimation against modeling and measurement errors by considering the balance among these errors from the motor side, transmission part, and torque sensor;

(2) systematic design of the gains determining the balance for minimum variance estimation;

(3) performance evaluation through simulations and experiments.

This study extends previous developments [23–25] by added discussion and improved experimental results. The remaining of this paper is organized as follows. The experimental setup is described in section 2. In section 3, the proposed observer is detailed. In section 4, the systematic design for the gains to enhance robustness is proposed, and the variance minimization of the estimated load-side external torque is determined. The performance of the proposed method is analyzed through simulations and experiments in sections 3 and 4. Finally, we draw conclusions in section 5.

## 2. Experimental setup

A motor bench with a low-stiffness joint between two mo-

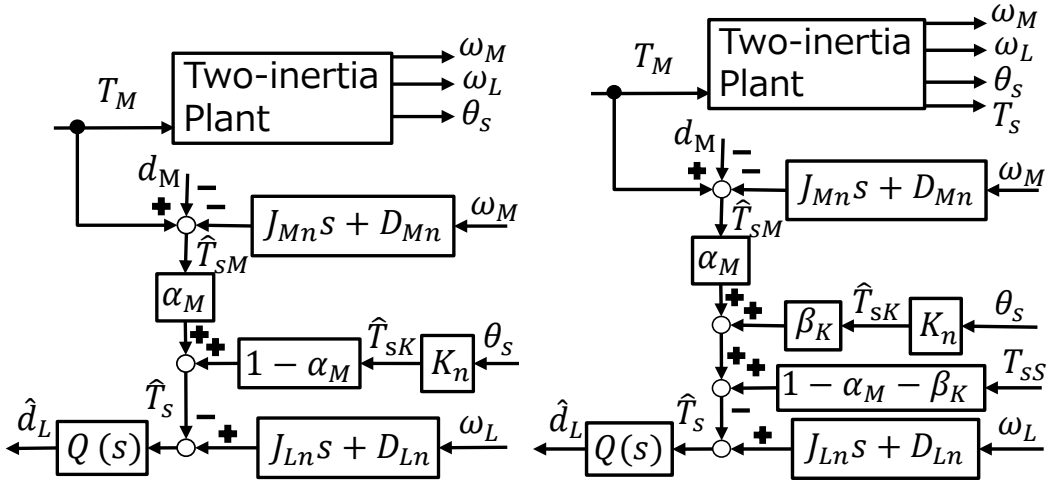


(a) The proposed load-side external torque observer without a joint torque sensor.

(b) The proposd load-side external torque observer with a joint torque sensor.

Fig. 3. Block diagrams of the proposed load-side external torque observers with/without a joint torque sensor.

tors is used as two-inertia system for this study by adopting the setup shown in Fig. 2. Its angular velocities can be accurately measured with 20-bit high-resolution encoders on both the motor and load sides. A flexible joint between the motor and load is inserted to reduce the torsional rigidity.

We implement the controllers on a digital signal processor. The sampling frequency of the proportional–integral current control loop is 10 kHz with an experimentally determined bandwidth of 1.2 kHz. The motor torque is measured by a previously determined torque constant value, $K_t$=0.172 N·m/A, multiplied by the measured current obtained from a sensor.

We measure the frequency response by feeding chirp signals as current reference. The responses from the motor torque to the motor angle and from the motor torque to the load angle are shown in Figs. 1(b) and 1(c), respectively. The responses verify that the experimental setup can be modeled as a two-inertia system whose antiresonance and resonance frequencies are 57 and 71 Hz, respectively. The resulting model is depicted with blue solid lines, whereas measurement results are depicted with red dashed lines. The parameters identified for the model are listed in Table 2.

## 3. Proposed load-side external torque estimation

**3.1 Observer** The motor and load angular velocities and the torsional angle can be measured using the corresponding encoders. First, we consider no joint torque sensor available. Assuming a stepwise load-side external torque $\dot{d}_L = 0$, the augmented state equation of the plant is expressed as:

$$\begin{bmatrix} \dot{\omega}_M \\ \dot{\omega}_L \\ \dot{\theta}_s \\ \dot{d}_L \end{bmatrix} = \begin{bmatrix} -\frac{D_M}{J_M} & 0 & -\frac{K}{J_M} & 0 \\ 0 & -\frac{D_L}{J_L} & \frac{K}{J_L} & \frac{1}{J_L} \\ 1 & -1 & 0 & 0 \\ 0 & 0 & 0 & 0 \end{bmatrix} \begin{bmatrix} \omega_M \\ \omega_L \\ \theta_s \\ d_L \end{bmatrix} + \begin{bmatrix} \frac{1}{J_M} \\ 0 \\ 0 \\ 0 \end{bmatrix} T_M,$$

$$y = \begin{bmatrix} 1 & 0 & 0 & 0 \\ 0 & 1 & 0 & 0 \\ 0 & 0 & 1 & 0 \end{bmatrix} \begin{bmatrix} \omega_M \\ \omega_L \\ \theta_s \\ d_L \end{bmatrix}. \tag{4}$$

Then, a first-order minimal-order observer estimating $d_L$ is introduced as (5), where $z$ is a scalar state variable of the observer and $L = [l_1,\ l_2,\ l_3]$ is the observer gain vector.

$$\begin{aligned} &\dot{z} = A_r z + B_r T_M + F_r y, \quad \hat{d}_L = z + Ly, \\ &A_r = -\frac{l_2}{J_{Ln}}, \quad B_r = -\frac{l_1}{J_{Mn}}, \\ &F_r = \begin{bmatrix} f_{r1} & f_{r2} & f_{r3} \end{bmatrix}, \\ &f_{r1} = -\frac{1}{J_{Ln}} l_1 l_2 + \frac{D_{Mn}}{J_{Mn}} l_1 - l_3, \\ &f_{r2} = -\frac{1}{J_{Ln}} l_2^2 + \frac{D_{Ln}}{J_{Ln}} l_2 + l_3, \\ &f_{r3} = -\frac{1}{J_{Ln}} l_2 l_3 + K_n \left( \frac{1}{J_{Mn}} l_1 - \frac{1}{J_{Ln}} l_2 \right). \end{aligned} \tag{5}$$

To analyze the physical meaning of the observer given by (5), it is convenient to represent it as a block diagram. Then, the equivalent conversion of the block diagram results in that shown in Fig. 3(a), whose variables are defined as follows:

$$Q(s) = \frac{\frac{l_2}{J_{Ln}}}{s + \frac{l_2}{J_{Ln}}}, \tag{6}$$

$$\alpha_M = \frac{J_{Ln}}{J_{Mn}} \frac{l_1}{l_2}. \tag{7}$$

The first-order low-pass filter, $Q(s)$, determines the estimation bandwidth, i.e., the bandwidth is defined by observer gain $l_2$, and $\alpha_M$ determines the ratio between $\hat{T}_{sM}$ and $\hat{T}_{sK}$ as follows:

$$\hat{T}_s = \alpha_M \hat{T}_{sM} + (1 - \alpha_M) \hat{T}_{sK}. \tag{8}$$

Equation (8) indicates that $\alpha_M$ can be designed considering the accuracy of $\hat{T}_{sM}$ and $\hat{T}_{sK}$, where the former depends on the accuracy of motor parameters and friction model, whereas the latter depends on the accuracy of torsional rigidity and nonlinear models when nonlinearities in transmission mechanisms such as backlash exist. Given that $l_2$ is experimentally selected according to the desired bandwidth and stable margin, $\alpha_M$ is designed by observer gain $l_1$ and indicates

the amount of motor-side information that is used. Specifically, when $\alpha_M$ is 1 (i.e., $l_1$ is $\frac{J_{Mn}}{J_{Ln}} l_2$), the proposed observer is equivalent to the estimation proposed in [14], whereas when $\alpha_M$ is 0 (i.e., $l_1$ is 0), the proposed observer is equivalent to the estimation proposed in [15]. Therefore, the proposed load-side external torque observer extends these conventional observers by including them as particular cases.

When the system has a joint torque sensor, the minimal-order observer can be derived in the same way as (4)–(7). The state vector is changed from $\boldsymbol{x} = [\omega_M,\ \omega_L,\ \theta_s,\ d_L]^{\mathrm{T}}$ to $\boldsymbol{x} = [\omega_M,\ \omega_L,\ T_s,\ d_L]^{\mathrm{T}}$ to realize a minimal-order observer since the joint torque is measurable by a joint torque sensor. Then, the joint torque is estimated by introducing a gain $\beta_K$, which determines how much the torsional information is used as follows:

$$\hat{T}_s = \alpha_M \hat{T}_{sM} + \beta_K \hat{T}_{sK} + (1 - \alpha_M - \beta_K) T_{sS} . \cdots\cdots\cdots (9)$$

Here, $\alpha_M$ and $\beta_K$ determine the ratio among the motor-side estimation, the transmission-part estimation, and the joint torque sensor measurement. The block diagram is shown in Fig. 3(b). This is a simple expansion of Fig. 3(a) by the additional use of the joint torque sensor information.

**3.2 Gain evaluation through simulations** We conduct simulations and experiments without using a joint torque sensor for load-side torque estimation. In addition, we consider no motor disturbance during simulations, i.e., $d_M = 0$, and no nonlinearity in the transmission mechanisms. The cut-off frequency of $Q(s)$ is experimentally determined to be 150 Hz.

Our theoretical analyses indicate a sensitivity tradeoff between motor and transmission modeling errors depending on $\alpha_M$. Figure 4(a) shows the estimated external torque responses when the motor has modeling errors ($J_M = 1.5J_{Mn}$, $D_M = 1.5D_{Mn}$) for a 2.0 N·m torque step applied to $d_L$ at 0.050 s, as indicated in the black dotted line. When $\alpha_M = 0$, the estimated response shows an ideal low-pass characteristic without deterioration by modeling errors of motor parameters. Figure 4(a) shows that the estimation accuracy increases for smaller values of $\alpha_M$. Figure 4(b) shows the estimated external torque when the transmission has modeling errors ($K = 1.5K_n$). When $\alpha_M = 1$, the estimated response shows an ideal low-pass characteristic without deterioration by modeling errors of transmission parameters, and the estimation accuracy increases as $\alpha_M$ approaches 1. Figure 4(c) shows the estimation errors in Figs. 4(a) and 4(b). The vertical axis in Fig. 4(c) corresponds to the one-second integral of the estimation error, i.e., $\int_{0.050}^{1.050} (d_{LRef} - \hat{d}_L) dt$, and $d_{LRef}$ is the input load-side external torque denoted as Ref in Figs. 4(a) and 4(b). Clearly, small $\alpha_M$ values reduce the influence of motor model errors, and $\alpha_M$ approaching 1 reduces the influence of transmission model errors.

In practice, every plant parameter has errors, and in some cases the transmission model can be assumed to present either smaller or larger errors than the motor model. Then, $\alpha_M$ can be selected for more accurate estimation considering the balance between the model parameter errors between the motor and transmission. Figure 5(a) shows the estimated torque when larger modeling error is attributed to the motor than to the transmission model. Specifically, +50% error is set to the motor viscosity and +20% error to the torsional rigidity (i.e., $D_M = 1.5D_{Mn}$, $K = 1.2K_n$). Moreover, a −0.50 N·m step motor torque disturbance is applied at 0.20 s. As a large modeling error is given to the motor parameters, better responses are obtained as $\alpha_M$ approaches 0. In fact, small $\alpha_M$ values retrieve a gradual decrease by $D_M$ error, and the effect of the sudden decrease by $d_M$ is mitigated for the estimated external torque. In contrast, vibration induced by the torsional rigidity modeling error increases for small $\alpha_M$ values. Figure 5(b) shows the torque estimation when larger modeling error is attributed to the transmission than to the motor model. Hence, +20% error is set to the motor viscosity and +50% error to the torsional rigidity (i.e., $D_M = 1.2D_{Mn}$, $K = 1.5K_n$). The graph confirms that the estimation accuracy improves as $\alpha_M$ approaches 1. The simulation results suggest that the proposed load-side external torque observer enables more accurate estimation than conventional observers provided that gain $\alpha_M$ is adequately designed.

**3.3 Gain evaluation through experiments** We confirm the simulation results shown in Figs. 5(a) and 5(b) through experiments. The designed observer is discretized by the Tustin transformation with sampling frequency of 2.5 kHz and load-side external torque $d_L$ input by the load-side motor. Modeling error is introduced by varying the observer parameters (e.g., $D'_{Mn} = D_{Mn}/1.5$) instead of the plant parameters. Therefore, the conditions in the experiments are different from those of the simulations, but similar results are expected. Figure 6(a) shows the estimated response when $D'_{Mn} = D_{Mn}/1.5$ and $K'_n = K_n/1.2$. The large modeling error on the motor-side parameters makes the estimation accuracy improve as $\alpha_M$ approaches 0. When $\alpha_M = 0$, both the decrease in the estimated torque caused by modeling error in $D_M$ and the influence of $d_M$ at 0.20 s are removed. Figure 6(b) shows the estimated torque when $D'_{Mn} = D_{Mn}/1.2$ and $K'_n = K_n/1.5$. As expected, the estimation accuracy improves as $\alpha_M$ approaches 1 because a larger error is present in the transmission model. In both cases, the experimental results confirm the simulation outcomes, thus validating the proposed observer.

## 4. Proposed minimum variance estimation

**4.1 Gain design** In the previous section, we demonstrate that the estimation accuracy can be changed according to the value of the gain and the accuracy of plant parameters. Instead of manual adjustment, a systematic design for the gain is more suitable in practical settings. In this section, we propose a gain design method to minimize the variance for estimating $d_L$ assuming that the range of plant parameter variations is known. This is a valid assumption as a variation from the nominal values of plant parameters (e.g., motor inertia moment, viscosity, and torsional rigidity change up to ±5%, ±30%, and ±20%, respectively) can be often assumed. To determine $\alpha_M$, it is also assumed that the plant parameters follow a Gaussian probability distribution and are independent from each other. Each distribution has mean $\mu$, which is equal to the nominal value of the parameter, and variance $\sigma^2$, which depends on the reliability of each parameter. For instance, if the torsional rigidity is assumed to change from 0.80 to 1.20 of the nominal value within 99.7% probability, variance $\sigma^2$ can be obtained as $3\sigma^2$=0.20$\mu$.

In the proposed observer, $d_L$ is estimated as:

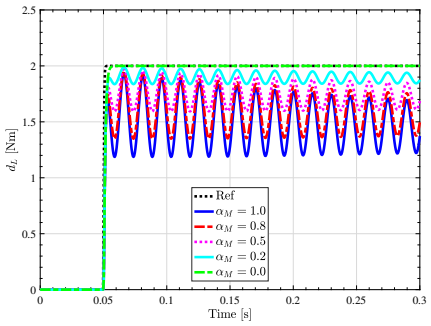


(a) Case1:$J_M = 1.5J_{Mn}$, $D_M = 1.5D_{Mn}$ with various $\alpha_M$.

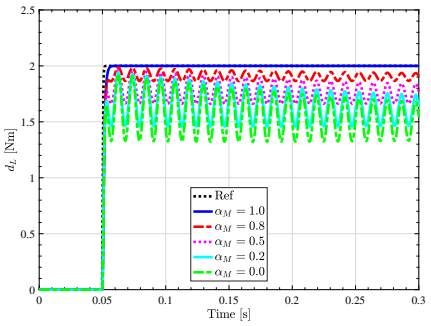


(b) Case2:$K = 1.5K_n$ with various $\alpha_M$.

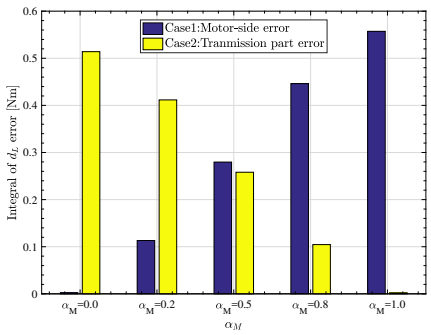


(c) Comparison of the integral of the estimation errors in the left two cases.

Fig. 4. Comparison of the errors when $JM = 1.5J_{Mn}$ and $D_M = 1.5D_{Mn}$, or $K = 1.5K_n$, with various $\alpha_M$.

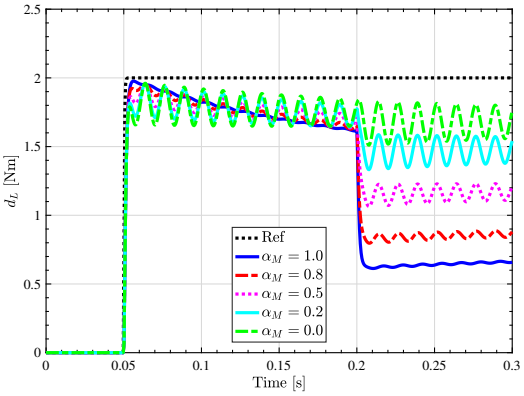


(a) Larger error in motor side than transmission part: $D_M = 1.5D_{Mn}$, $K = 1.2K_n$.

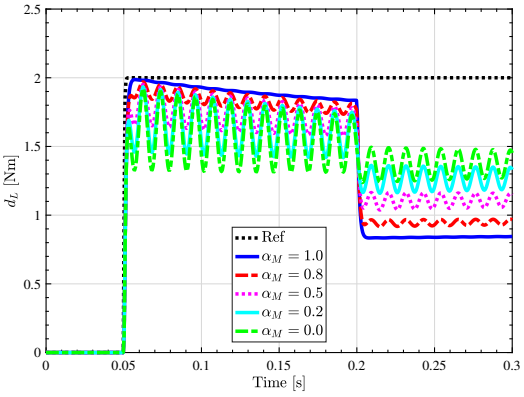


(b) Larger error in transmission part than motor side: $D_M = 1.2D_{Mn}$, $K = 1.5K_n$.

Fig. 5. Simulation comparison of load-side external torque responses in two cases, and -1.0 N·m step $d_M$ is input at 0.20 s with various $\alpha_M$.

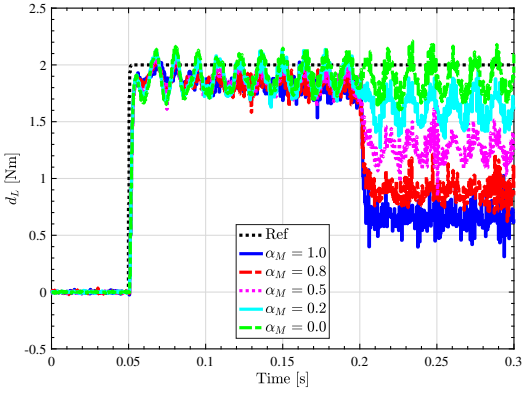


(a) Larger error in motor side than transmission part: $D'_{Mn} = D_{Mn}/1.5$, $K'_n = K_n/1.2$.

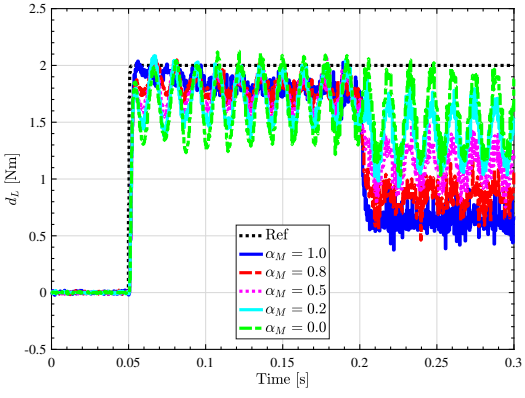


(b) Larger error in transmission part than motor side:$D'_{Mn} = D_{Mn}/1.2$, $K'_n = K_n/1.5$.

Fig. 6. Experimental comparison of load-side external torque responses in two cases, and -1.0 N·m step $d_M$ is input at 0.20 s with various $\alpha_M$.

$$\hat{d}_L = (J_{Ln}s + D_{Ln})\omega_L - \alpha_M \hat{T}_{sM} - (1-\alpha_M)\hat{T}_{sK}. \quad (10)$$

and $\alpha_M$ should be designed to minimize the variance of $\hat{d}_L$. The estimation variance can be calculated as:

$$\begin{aligned}\sigma^2_{\hat{d}_L} &= \sigma^2_L + \alpha^2_M \sigma^2_{\hat{T}_{sM}} + (1-\alpha_M)^2 \sigma^2_{\hat{T}_{sK}} \\ &= (\sigma^2_{\hat{T}_{sM}} + \sigma^2_{\hat{T}_{sK}}) \left( \alpha_M - \frac{\sigma^2_{\hat{T}_{sK}}}{\sigma^2_{\hat{T}_{sM}} + \sigma^2_{\hat{T}_{sK}}} \right)^2 \\ &\quad + \frac{\sigma^2_{\hat{T}_{sM}} \sigma^2_{\hat{T}_{sK}}}{\sigma^2_{\hat{T}_{sM}} + \sigma^2_{\hat{T}_{sK}}} + \sigma^2_L, \end{aligned} \quad (11)$$

where $\sigma^2_{\hat{d}_L}$, $\sigma^2_L$, $\sigma^2_{\hat{T}_{sM}}$, and $\sigma^2_{\hat{T}_{sK}}$ are the variances of $d_L$, load-side, motor-side, and transmission-part estimations, respectively. Equation (11) indicates that $\sigma^2_{\hat{d}_L}$ can be minimized using the following $\alpha_M$:

$$\alpha_M = \frac{\sigma^2_{\hat{T}_{sK}}}{\sigma^2_{\hat{T}_{sM}} + \sigma^2_{\hat{T}_{sK}}}. \quad (12)$$

$$\sigma^2_{\hat{d}_{LS}} = (\sigma^2_{\hat{T}_{sM}} + \sigma^2_{\hat{T}_{sS}})\left(\alpha_M - \frac{\sigma^2_{\hat{T}_{sS}}}{\sigma^2_{\hat{T}_{sM}} + \sigma^2_{\hat{T}_{sS}}}(1-\beta_K)\right)^2 + \frac{\sigma^2_{\hat{T}_{sM}}\sigma^2_{\hat{T}_{sK}} + \sigma^2_{\hat{T}_{sK}}\sigma^2_{\hat{T}_{sS}} + \sigma^2_{\hat{T}_{sS}}\sigma^2_{\hat{T}_{sM}}}{\sigma^2_{\hat{T}_{sM}} + \sigma^2_{\hat{T}_{sS}}}\left(\beta_K - \frac{\sigma^2_{\hat{T}_{sS}}\sigma^2_{\hat{T}_{sM}}}{\sigma^2_{\hat{T}_{sM}}\sigma^2_{\hat{T}_{sK}} + \sigma^2_{\hat{T}_{sK}}\sigma^2_{\hat{T}_{sS}} + \sigma^2_{\hat{T}_{sS}}\sigma^2_{\hat{T}_{sM}}}\right)^2 + \frac{\sigma^2_{\hat{T}_{sM}}\sigma^2_{\hat{T}_{sK}}\sigma^2_{\hat{T}_{sS}}}{\sigma^2_{\hat{T}_{sM}}\sigma^2_{\hat{T}_{sK}} + \sigma^2_{\hat{T}_{sK}}\sigma^2_{\hat{T}_{sS}} + \sigma^2_{\hat{T}_{sS}}\sigma^2_{\hat{T}_{sM}}} + \sigma^2_L, \quad (17)$$

Then, $\sigma^2_{\hat{T}_{sM}}$ and $\sigma^2_{\hat{T}_{sK}}$ can be calculated by linear approximation of (2) and (3):

$$\sigma^2_{\hat{T}_{sM}} = \dot{\omega}_M^2\sigma^2_{J_M} + \omega_M^2\sigma^2_{D_M} + J^2_{Mn}\sigma^2_{\dot{\omega}_M} + D^2_{Mn}\sigma^2_{\omega_M} + \sigma^2_{T_M} + \sigma^2_{d_M}, \quad (13)$$

$$\sigma^2_{\hat{T}_{sK}} = (\theta_M - \theta_L)^2\sigma^2_K + K_n^2\sigma^2_{\theta_M} + K_n^2\sigma^2_{\theta_L}, \quad (14)$$

where $\sigma^2_{J_M}$, $\sigma^2_{D_M}$, $\sigma^2_K$, $\sigma^2_{T_M}$, and $\sigma^2_{d_M}$ are the variances of the corresponding parameter. The variation of measured motor torque $\sigma^2_{T_M}$ is caused by current sensor noise. Here please note that the nonlinear effects such as motor Coulomb friction and backlash are not considered explicitly but it can be included. Motor Coulomb friction can be considered in the variance of motor-side disturbance $\sigma^2_{d_M}$ and the backlash in the variance of torsional rigidity $\sigma^2_K$. Also, $\sigma^2_{\theta_M}$, $\sigma^2_{\theta_L}$, $\sigma^2_{\omega_M}$, and $\sigma^2_{\dot{\omega}_M}$ are the measurement variances, which are caused by the quantization error from the encoder. When the resolution of the encoder is $q$, its variance is calculated as:

$$\sigma^2(q) = \int_{-\frac{q}{2}}^{\frac{q}{2}} \frac{1}{q}x^2dx = \frac{q^2}{12}. \quad (15)$$

When the angular velocity and angular acceleration are obtained by backward difference, their resolutions are calculated as $\omega_{res}(q) = \frac{q}{T_s}$ and $\dot{\omega}_{res}(q) = \frac{q}{T_s^2}$, respectively, where $T_s$ is the sampling time. Therefore, the variances of the encoder measurements can be calculated by substituting the resolutions into (15).

The proposed method can be extended to consider a joint torque sensor, whose block diagram is shown in Fig. 3(b). The sensor is robust against modeling errors but suffers from noise. Therefore, combining the three obtained joint torques, $\hat{T}_{sM}$, $\hat{T}_{sK}$, and $T_{sS}$, can improve the estimation accuracy. Gains $\alpha_M$ and $\beta_K$ can be designed to minimize the variance of the estimated $d_L$.

The noise of the joint torque sensor is also assumed to follow a Gaussian probability distribution. In the proposed observer with the sensor, $d_L$ is estimated as:

$$\begin{aligned}\hat{d}_L =&(J_{Ln}s + D_{Ln})\omega_L \\ &- \alpha_M\hat{T}_{sM} - \beta_K\hat{T}_{sK} - (1-\alpha_M-\beta_K)T_{sS}. \end{aligned} \quad (16)$$

The estimation variance can be calculated as (17): where $\sigma^2_{\hat{d}_{LS}}$ and $\sigma^2_{T_{sS}}$ are the variance of $d_L$ estimation with joint torque sensor and that of the sensor measurement, respectively. Therefore, $\sigma_{\hat{d}_{LS}}$ can be minimized using the following $\alpha_M$ and $\beta_K$:

$$\alpha_M = \frac{\sigma^2_{\hat{T}_{sK}}\sigma^2_{\hat{T}_{sS}}}{\sigma^2_{\hat{T}_{sM}}\sigma^2_{\hat{T}_{sK}} + \sigma^2_{\hat{T}_{sK}}\sigma^2_{\hat{T}_{sS}} + \sigma^2_{\hat{T}_{sS}}\sigma^2_{\hat{T}_{sM}}}, \quad (18)$$

$$\beta_K = \frac{\sigma^2_{\hat{T}_{sS}}\sigma^2_{\hat{T}_{sM}}}{\sigma^2_{\hat{T}_{sM}}\sigma^2_{\hat{T}_{sK}} + \sigma^2_{\hat{T}_{sK}}\sigma^2_{\hat{T}_{sS}} + \sigma^2_{\hat{T}_{sS}}\sigma^2_{\hat{T}_{sM}}}. \quad (19)$$

Comparing the proposed method with and without joint torque sensor shows that the variance of the estimated $d_L$ always reduces using the joint torque sensor:

$$\begin{aligned}&\sigma^2_{\hat{d}_L} - \sigma^2_{\hat{d}_{LS}} \\ &= \frac{\sigma^2_{\hat{T}_{sS}}\sigma^2_{\hat{T}_{sM}}}{(\sigma^2_{\hat{T}_{sM}} + \sigma^2_{\hat{T}_{sK}})(\sigma^2_{\hat{T}_{sM}}\sigma^2_{\hat{T}_{sK}} + \sigma^2_{\hat{T}_{sK}}\sigma^2_{\hat{T}_{sS}} + \sigma^2_{\hat{T}_{sS}}\sigma^2_{\hat{T}_{sM}})} \\ &\geq 0. \end{aligned} \quad (20)$$

Note that besides the variance reduction, the estimation accuracy is not influenced by the error of nominal parameters when using a joint torque sensor, as $T_{sS}$ can be obtained with robustness against modeling errors of the nominal parameters.

**4.2 Minimum variance evaluation through simulations** The simulations and experiments for minimum variance estimation consider six methods: only motor-side encoder estimation based on state observer, motor-side estimation based on (2), transmission-part estimation based on (3), proposed estimation without joint torque sensor based on (8), torque-sensor-based estimation based on $T_{sS}$, and proposed estimation with joint torque sensor based on (9). The load-side external torque can be estimated only using the motor-side encoder by implementing the state observer. Assuming a stepwise load external torque $\dot{d}_L = 0$, it can be estimated from the augmented state vector. Given that the state observer using only the motor-side encoder requires all plant parameters, it is severely affected by modeling errors. The sensor configurations for the six evaluated methods are listed in Table 3.

To compare the performance of each method, we evaluated the variance and $L_2$ norm error of the load-side external torque through simulations. The $L_2$ norm error is analyzed to evaluate the robustness against the nominal model error (i.e., $\mu$ error in Gaussian probability distribution). A 1.0 N·m step load-side external torque was input to the six estimation methods undergoing plant parameter variations. We conducted 10000 simulation trials per method and averaged the variance and $L_2$ norm error of the load-side external torque.

The motor and transmission model parameters were randomly chosen from their probability distributions in each simulation, and the joint torque sensor measurement noise also followed the corresponding Gaussian probability distribution. The $3\sigma^2$ plant parameter variation in the simulated plant is given as follows: $J_M$:±5%, $D_M$:±50%, $K$:±30%, $d_M$:±0%. The variances of plant parameters, $\sigma^2_{J_M}$, $\sigma^2_{D_M}$, $\sigma^2_K$, and $\sigma^2_{d_M}$, in $\alpha_M$ and $\beta_K$ design were based on these variations, and those of encoder measurements, $\sigma^2_{\theta_M}$, $\sigma^2_{\theta_L}$, $\sigma^2_{\omega_M}$, and $\sigma^2_{\dot{\omega}_M}$, were given for a 20-bit resolution according to (15). In addition, the variance of the torque sensor was determined assuming that 99.7% of the torque sensor noise lies within the 1.0% of the rated measurable torque (20 N·m). Therefore, $3\sigma^2_{T_{sS}} = 20 \cdot 0.010$. Also, the motor torque measurement variation caused by current sensor noise can be designed by measuring the noise as joint torque sensor. In this paper, $\sigma^2_{T_M}$ is designed to be zero since motor torque is not input in our

Table 3. Sensor configurations in six estimation methods.

| | motor-side encoder | load-side encoder | joint torque sensor |
|---|---|---|---|
| Only motor-side encoder estimation | ✓ | | |
| Motor-side estimation | ✓ | ✓ | |
| Transmission-part estimation | ✓ | ✓ | |
| Prop. w/o torque sensor | ✓ | ✓ | |
| Torque-sensor-based estimation | | ✓ | ✓ |
| Prop. w/i torque sensor | ✓ | ✓ | ✓ |

Table 4. Statistical analyses in simulations.

| | Variance | $L_2$ norm error |
|---|---|---|
| Only motor-side encoder | 8.8e-3 | 1.1e+2 |
| Motor-side | 1.2e-3 | 3.0e+1 |
| Transmission-part | 1.5e-3 | 4.4e+1 |
| Prop. w/o torque sensor | 1.0e-3 | 1.8e+1 |
| Torque-sensor-based | 9.8e-4 | 9.8 |
| Prop. w/i torque sensor | 9.4e-4 | 1.4e+1 |

simulation and experimental scenarios.

Table 4 lists the estimation performance of the six evaluated methods. In the estimation based only on the motor-side encoder, the variance and error of the estimated torque are much larger than those from the other methods, thus indicating the clear advantage of applying a load-side encoder for external torque estimation. In our proposed method without joint torque sensor, the variance reduces compared to both the motor-side and transmission-part estimation, despite the sensor configurations of the three methods being the same. Our method without torque sensor can reduce the variance and $L_2$ norm error by using the plant parameter and measurement information (i.e., the variance of the Gaussian probability distribution). Compared with the torque-sensor-based estimation, the variance in our previous proposed method is larger, because the variance of the torque sensor measurement was small in this simulation.

When the system has a joint torque sensor, the proposed method further reduces the estimation variance to the smallest value among the evaluated methods. Still, regarding the $L_2$ norm error, our method is inferior to the torque-sensor-based estimation, because the proposed method determines gains $\alpha_M$ and $\beta_K$ that minimize the variance instead of the $L_2$ norm error. Moreover, as the model parameters of the motor and transmission ($J_M$, $D_M$, and $K$) varied during simulation, the torque-sensor-based estimation retrieves a smaller $L_2$ norm error as it is not influenced by the parameter variation. In practice, however, the torque sensor measurements do not follow the Gaussian probability distribution by the presence of offset, drift, and hysteresis, resulting in deterioration of the estimation accuracy. The experimental results presented in the sequel show this deterioration by unmodeled effects of the torque sensor.

**4.3 Minimum variance evaluation through experiments** During the experiments to evaluate minimum variance estimation, we used the nominal plant parameters identified in section 2 for the observers. To select $\alpha_M$ and $\beta_K$, the variances of the plant parameters, $\sigma^2_{J_M}$, $\sigma^2_{D_M}$, $\sigma^2_K$, and $\sigma^2_{d_M}$, were set to $3\sigma^2$ of the parameters: $J_M$:±1%, $D_M$:±10%, $K$:±20%, and $d_M$:±0%. The variance of the joint torque sensor was determined based on the assumption that 99.7% of its noise lies within the 0.050% of the rated measurable torque. In addition, we removed the offset of the joint torque sensor

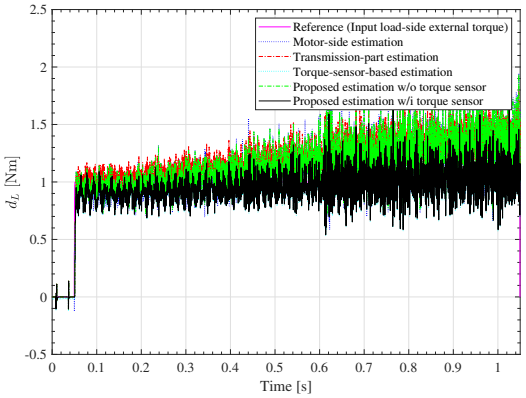


Fig. 7. Comparison of estimation performance in experiments.

Table 5. Experimental results.

| | Variance | $L_2$ norm error |
|---|---|---|
| Only motor-side encoder | 0.959 | 5.96e+3 |
| Motor-side | 0.219 | 4.21e+2 |
| Transmission-part | 0.226 | 4.49e+2 |
| Prop. w/o torque sensor | 0.218 | 4.07e+2 |
| Torque-sensor-based | 0.148 | 1.43e+2 |
| Prop. w/i torque sensor | 0.147 | 1.39e+2 |

measurements and applied a 1.0 N·m step load-side external torque for 1.0 s.

Figure 7 shows the comparison of the estimation performance. In Fig. 7, the response of only motor-side encoder estimation is not shown because the response is too noisy. The variance and $L_2$ norm error of the proposed estimation method are listed in Table 5. The tendency of the experimental results are similar to that of the simulation results shown in Table 4. Using only the motor-side encoder, it is difficult to determine an accurate estimation. Still, the proposed methods show the smallest variance and errors for the same sensor configuration. Unlike simulation, the $L_2$ norm error of the proposed method with joint torque sensor was smaller than that of the torque-sensor-based estimation in the experiments. This opposite trend is likely to be caused by the nonlinearities of the torque sensor signal. Although the real measurements from the joint torque sensor deteriorate the estimation accuracy, the proposed method improves estimation by combining the information from both encoders.

## 5. Conclusion

By analyzing the minimal-order observer for load-side external torque estimation, we propose an improved observer. The proposed method combines two conventional observers for increased estimation accuracy by considering the modeling and measurement errors in the motor and transmission of a two-inertia system. Furthermore, we propose a load-side

external torque observer considering a joint torque sensor, which notably improves the robustness against modeling errors. Then, for minimum variance estimation of load-side external torque, we derive a systematic design for the observer gains based on the variance of the plant parameters and measurements assuming that they follow independent Gaussian probability distributions. Simulation and experimental results verify the high performance of the proposed observers compared to similar methods. To further improve the estimation accuracy, we will investigate the online identification of load-side parameters in a future development.

## References


( 1 ) S. Lee, Y. Yamada, K. Ichikawa, O. Matsumoto, K. Homma, and E. Ono: "Safety-Function Design for the Control System of a Human-Cooperative Robot Based on Functional Safety of Hardware and Software", *IEEE/ASME Trans. Mechatronics*, Vol. 19, No. 2, pp. 719–729 (2014)

( 2 ) Y. Yamada and Y. Kakinuma: "Sensorless cutting force estimation for full-close controlled ball-screw-driven stage", *The Int. J. Advanced Manufacturing Technology*, Vol. 87, No. 9, pp. 3337–3348 (2016)

( 3 ) Y. Ohba, M. Sazawa, K. Ohishi, T. Asai, K. Majima, Y. Yoshizawa, and K. Kageyama: "Sensorless Force Control for Injection Molding Machine Using Reaction Torque Observer Considering Torsion Phenomenon", *IEEE Trans. Ind. Electron.*, Vol. 56, no. 8, pp. 2955–2960 (2009)

( 4 ) S. Katsura and K. Ohnishi: "Force Servoing by Flexible Manipulator Based on Resonance Ratio Control", *IEEE Trans. Ind. Electron.*, Vol. 54, No. 1, pp. 539–547 (2007)

( 5 ) C. Mitsantisuk, M. Nandapaya, K. Ohishi, and S. Katsura: "Design for Sensorless Force Control of Flexible Robot by Using Resonance Ration Control Based on Coefficient Diagram Method", *Automatika*, Vol. 54, No. 1, pp. 62–73 (2013)

( 6 ) Y. Asai, Y. Yokokura, and K. Ohishi: "Fine Force Reproduction of Environmental Haptic Sensations Based on Momentum Control", *IEEE Trans. Ind. Electron.*, Vol. 63, No. 7, pp. 4304–4313 (2016)

( 7 ) T. Tsuji, T. Seki, and S. Sakaino: "Intrinsic Contact Sensing for Touch Interface With Movable Structure", *IEEE Trans. Ind. Electron.*, Vol. 64, No. 9, pp. 7342–7349 (2017)

( 8 ) S. Fukushima, H. Sekiguchi, Y. Saito, W. Iida, T. Nozaki, and K. Ohnishi: "Artificial Replacement of Human Sensation Using Haptic Transplant Technology", *IEEE Trans. Ind. Electron.*, Vol. 65, No. 5, pp. 3985–3994 (2018)

( 9 ) S. Oh, K. Kong, and Y. Hori: "Design and Analysis of Force-Sensor-Less Power-Assist Control", *IEEE Trans. Ind. Electron.*, Vol. 61, No. 2, pp. 985–993 (2014)

(10) T. Murakami, F. Yu, and K. Ohnishi: "Torque sensorless control in multidegree-of-freedom manipulator", *IEEE Trans. Ind. Electron.*, Vol. 40, No. 2, pp. 259–265 (1993)

(11) K. Szabat and T. Orlowska-Kowalska: "Vibration Suppression in a Two-Mass Drive System Using PI Speed Controller and Additional Feedbacks–Comparative Study", *IEEE Trans. Ind. Electron.*, Vol. 54, No. 2, pp. 1193–1206 (2007)

(12) Y. Kuroki, Y. Kosaka, T. Takahashi, E. Niwa, H. Kaminaga, and Y. Nakamura: "Cr–N Alloy Thin–film Based Torque Sensors and Joint Torque Servo Systems for Compliant Robot Control", *Proc. IEEE Int. Conf. on Robotics and Automation (ICRA)*, pp. 4954–4959 (2013)

(13) S. Yamada, K. Inukai, H. Fujimoto, K. Omata, Y. Takeda, and S. Makinouchi: "Joint torque control for two-inertia system with encoders on drive and load sides", *Proc. of the 13th IEEE Int. Conf. Ind. Informat. (INDIN)*, pp. 396–401 (2015)

(14) M. Matsuoka, T. Murakami, and K. Ohnishi: "Vibration suppression and disturbance rejection control of a flexible link arm", *Proc. of the Annu. Conf. of IEEE Ind. Electron. Soc. (IECON)*, pp. 1260–1265 (1995)

(15) J. Suzuki, T. Murakami, and K. Ohnishi: "Position and force control of flexible manipulator with position sensitive device", *Proc. of the 7th Int. Workshop on Advanced Motion Control (AMC)*, pp. 414–419 (2002)

(16) H. Zhang, S. Ahmad, and G. Liu: "Torque Estimation for Robotic Joint With Harmonic Drive Transmission Based on Position Measurements", *IEEE Trans. Robot.*, Vol. 31, No. 2, pp. 322–330 (2015)

(17) M. Nordin and P. Gutman: "Controlling mechanical systems with backlash –a survey", *Automatica*, Vol. 38, No. 10, pp. 1633-1649, Oct. 2002.

(18) M. Ruderman and M. Iwasaki: "Sensorless Torsion Control of Elastic-Joint Robots With Hysteresis and Friction", *IEEE Trans. Ind. Electron.*, Vol. 63, No. 3, pp. 1889–1899, Mar. 2016.

(19) E. Sariyildiz, G. Chen, and H. Yu: "An Acceleration-Based Robust Motion Controller Design for a Novel Series Elastic Actuator", *IEEE Trans. Ind. Electron.*, Vol. 63, No. 3, pp. 1900–1910 (2016)

(20) S. Oh and K. Kong: "High-Precision Robust Force Control of a Series Elastic Actuator", *IEEE/ASME Trans. Mechatronics*, Vol. 22, No. 1, pp. 71–80 (2017)

(21) C. Mitsantisuk, M. Nandapaya, K. Ohishi, and S. Katsura: "Parameter estimation of flexible robot using multi-encoder based on disturbance observer", *Proc. of the Annu. Conf. of IEEE Ind. Electron. Soc. (IECON)*, pp. 4424–4429 (2012)

(22) J. Lee, C. Lee, N. Tsagarakis, and S. Oh: "Residual-Based External Torque Estimation in Series Elastic Actuators Over a Wide Stiffness Range: Frequency Domain Approach", *IEEE Robot. Autom. Lett.*, Vol. 3 No. 3, pp. 1442–1449 (2018)

(23) S. Yamada and H. Fujimoto: "Precise External Torque Estimation for Two-Inertia System Considering Modeling Errors", *Proc. of the 2018 American Control Conf. (ACC)*, pp. 5238-5243 (2018)

(24) S. Yamada and H. Fujimoto: "Proposal of State-Dependent Minimum Variance Estimation of Load-Side External Torque Considering Modeling and Measurement Errors", *Proc. of the 27th IEEE International Symposium on Industrial Electronics (ISIE)*, pp. 1069–1074 (2018)

(25) S. Yamada and H. Fujimoto: "Minimum Variance Estimation of Load-side External Torque Using Load-side Encoder and Torque Sensor", The SICE Annual Conference 2018 (SICE 2018), pp. 737–742 (2018)



**Shota Yamada** (Student Member) received the B.S. and M.S. degree in the Department of Electrical Engineering and frontier sciences from The University of Tokyo in 2014 and 2016. He is currently working towards the Ph.D. degree in the Department of Electrical Engineering and Information systems at The University of Tokyo. He is also a research fellow (DC1) of Japan Society for the Promotion of Science from 2016. His research interests include force control, two-inertia system control.

**Hiroshi Fujimoto** (Senior Member) received the Ph.D. degree in the Department of Electrical Engineering from the University of Tokyo in 2001. In 2001, he joined the Department of Electrical Engineering, Nagaoka University of Technology, Niigata, Japan, as a research associate. From 2002 to 2003, he was a visiting scholar in the School of Mechanical Engineering, Purdue University, U.S.A. In 2004, he joined the Department of Electrical and Computer Engineering, Yokohama National University, Yokohama, Japan, as a lecturer and he became an associate professor in 2005. He is currently an associate professor of the University of Tokyo since 2010. He received the Best Paper Awards from the IEEE Transactions on Industrial Electronics in 2001 and 2013, Isao Takahashi Power Electronics Award in 2010, Best Author Prize of SICE in 2010, and The Nagamori Grand Award in 2016. His interests are in control engineering, motion control, nano-scale servo systems, electric vehicle control, motor drive, visual servoing, and wireless motors. Dr. Fujimoto is a member of the Society of Instrument and Control Engineers, the Robotics Society of Japan, and the Society of Automotive Engineers of Japan.